Environmental Pollution 276 (2021) 116708

Contents lists available at ScienceDirect

Environmental Pollution

journal homepage: www.elsevier.com/locate/envpol

Oxidation and sources of atmospheric NO*x* during winter in Beijing based on $\delta^{18}O$-$\delta^{15}N$ space of particulate nitrate☆

Zhongyi Zhang [a, b], Hui Guan [c], Hongwei Xiao [a], Yue Liang [a], Nengjian Zheng [a], Li Luo [a], Cheng Liu [a], Xiaozhen Fang [a], Huayun Xiao [d, *]

[a] Jiangxi Province Key Laboratory of the Causes and Control of Atmospheric Pollution, East China University of Technology, Nanchang, 330013, China
[b] School of Water Resources and Environmental Engineering, East China University of Technology, Nanchang, 330013, China
[c] The State Key Laboratory of Environmental Geochemistry, Institute of Geochemistry, Chinese Academy of Sciences, Guiyang, 550081, China
[d] School of Environmental Science and Engineering, Shanghai Jiao Tong University, Shanghai, 200240, China

ARTICLE INFO

Article history:
Received 6 July 2020
Received in revised form
2 February 2021
Accepted 5 February 2021
Available online 8 February 2021

Keywords:
Particulate nitrate
$\delta^{18}O$-$\delta^{15}N$ space
Vehicular exhaust
Beijing

ABSTRACT

The determination of both stable nitrogen ($\delta^{15}N{-}NO_3^-$) and stable oxygen ($\delta^{18}O{-}NO_3^-$) isotopic signatures of nitrate in $PM_{2.5}$ has shown potential for an approach of assessing the sources and oxidation pathways of atmospheric NO*x* (NO+NO_2). In the present study, daily $PM_{2.5}$ samples were collected in the megacity of Beijing, China during the winter of 2017–2018, and this new approach was used to reveal the origin and oxidation pathways of atmospheric NO*x*. Specifically, the potential of field $\delta^{15}N{-}NO_3^-$ signatures for determining the NO*x* oxidation chemistry was explored. Positive correlations between $\delta^{18}O{-}NO_3^-$ and $\delta^{15}N{-}NO_3^-$ were observed (with R^2 between 0.51 and 0.66, $p < 0.01$), and the underlying environmental significance was discussed. The results showed that the pathway-specific contributions to NO_3^- formation were approximately 45.3% from the OH pathway, 46.5% from N_2O_5 hydrolysis, and 8.2% from the NO_3+HC channel based on the $\delta^{18}O$-$\delta^{15}N$ space of NO_3^-. The overall nitrogen isotopic fractionation factor (εN) from NO*x* to NO_3^- on a daily scale, under winter conditions, was approximately +16.1‰±1.8‰ (consistent with previous reports). Two independent approaches were used to simulate the daily and monthly ambient NO*x* mixtures ($\delta^{15}N$-NO*x*), respectively. Results indicated that the monthly mean values of $\delta^{15}N$-NO*x* compared well based on the two approaches, with values of −5.5‰ ± 2.6‰, −2.7‰ ± 1.9‰, and −3.2‰ ± 2.2‰ for November, December, and January (2017–2018), respectively. The uncertainty was in the order of 5%, 5‰ and 5.2‰ for the pathway-specific contributions, the εN, and $\delta^{15}N$-NO*x*, respectively. Results also indicated that vehicular exhaust was the key contributor to the wintertime atmospheric NO*x* in Beijing (2017–2018). Our advanced isotopic perspective will support the future assessment of the origin and oxidation of urban atmospheric NO*x*.

1. Introduction

Haze pollution, characterized by exceedingly high mass loadings of fine particulate matter ($PM_{2.5}$: particles with an aerodynamic diameter smaller than 2.5 μm; from 100 to 1000 μg/m^3), has recently become one of the biggest concerns in most regions of China (An et al., 2019; Guo et al., 2014; Zhang et al., 2019; Huang et al., 2014). Elevated $PM_{2.5}$ concentrations can pose threats to air quality, global climate, and ecosystem health (An et al., 2019; Huang et al., 2014). More importantly, long-term exposure to elevated concentrations of $PM_{2.5}$ can impact the health of humans, and is estimated to have caused 1.1 million deaths in China in 2015 (An et al., 2019). High emissions of gaseous precursors (e.g., SO_2, NO*x*), efficient secondary particulate matter formation, and adverse meteorological conditions are assumed to play pivotal roles in haze development in China (An et al., 2019). The majority of the emitted SO_2 and NO*x* are converted into particulate sulfate (SO_4^{2-}) and nitrate (NO_3^-), respectively, by gas-phase reactions or multiphase chemistry in the atmosphere (Seinfeld and Pandis, 2016; Liu et al., 2020). To address severe haze pollution issues, the Chinese government has promoted numerous policies (e.g., the Air Pollution Prevention and Control Action Plan from 2013 to 2017) to reduce the emissions of SO_2 and NO*x* (Cheng et al., 2019; Zhang et al.,

☆ This paper has been recommended for acceptance by Admir C. Targino.
* Corresponding author.
E-mail address: xiaohuayun@ecut.edu.cn (H. Xiao).

https://doi.org/10.1016/j.envpol.2021.116708
0269-7491/

2019). Consequently, the annual mean $PM_{2.5}$ concentrations in Beijing declined from 89.5 μg/m^3 in 2013 to 58 μg/m^3 in 2017 (Zhou et al., 2019; Wang et al., 2019). Among the major inorganic species, SO_4^{2-} showed the largest reduction, with the mass contribution of SO_4^{2-} to $PM_{2.5}$ declining from 15.3% in 2013 to 10.7% in 2017 (Fu et al., 2020; Wang et al., 2019; Xu et al., 2019). In comparison, multi-year observations revealed that the winter NO_3^- concentrations have not decreased as expected, despite a reduction in the NO*x* mixing ratio by approximately 20% from 2013 to 2017 in Beijing (Fu et al., 2020; H. Li et al., 2019; Xu et al., 2019). In fact, high mass loadings of particulate NO_3^- (>40 μg/m^3) have recently been reported during haze pollution episodes in Beijing (Zhang et al., 2020a; Sun et al., 2020). Also, the mass contribution of NO_3^- to total $PM_{2.5}$ increased noticeably, from 12.7% in 2013 to 19.4% in 2017 (Cheng et al., 2019). As a consequence, the ratio of nitrate to sulfate (NO_3^-/SO_4^{2-}) has increased gradually in recent years (from 0.8 in 2013 to 1.5 in 2017) to be higher than 2.4 after 2018 (Sun et al., 2020; Fu et al., 2020; Wang et al., 2019). These results show that secondary NO_3^- now outweighs SO_4^{2-} and is playing an increasingly important role in particulate matter pollution. Understanding the major reaction pathways and the emission sources of NO*x* is not only a scientific mission, but it is also beneficial to the development of effective policies for alleviating nitrate haze pollution in the future.

NO*x* is emitted from natural sources (e.g., soil biogenic processes, lighting) and anthropogenic sources (e.g., coal combustion, vehicular exhaust, biomass burning) (Alexzander et al., 2020). Several common strategies have been used to apportion the NO*x* emission sources, e.g., atmospheric chemistry models, satellite observation, and nitrogen stable isotope techniques (Zong et al., 2020, and reference therein). However, previous studies based on diverse approaches (e.g., stable isotope tools, atmospheric chemistry models) highlighted large discrepancies in the NO*x* emission inventory in Beijing (Cheng et al., 2019; Li et al., 2017; Song et al., 2019a, 2019b; Zong et al., 2020). For example, atmospheric models and detailed local emission inventories (multi-resolution emission inventory for China (MEIC)) suggested that the transportation sector was the major contributor to the anthropogenic NO*x* emissions in Beijing from 2013 to 2017 (generally higher than 70%), while the contribution of other sectors (e.g., power and heating) decreased significantly during this period (Cheng et al., 2019). In contrast, the isotopic studies based on $\delta^{15}N-NO_3^-$ suggested that coal combustion was the primary source of NO*x* in Beijing from 2013 to 2018 (40%–60%), especially during winter seasons where energy is required for heating (Luo et al., 2019; Song et al., 2019a, 2019b; Zong et al., 2020; Fan et al., 2020).

The impacts of kinetic/equilibrium fractionation of NO*x* to NO_3^- on the $^{15}N/^{14}N$ ratios should be considered, when the implementation of source apportionment of NO*x* using $\delta^{15}N-NO_3^-$ (Chang et al., 2019; Elliott et al., 2019; Liu et al., 2020; Walters and Michalski, 2015a; Zhang et al., 2020c). For instance, the exchange equilibrium fractionation factor between NO and NO_2 (~40.3‰ at 278 K) can significantly influence the $\delta^{15}N$ signature of NO_2, and therefore the resultant NO_3^- (Walter et al., 2016). The transformation of NO*x* to HNO_3 and NO_3^- in the atmosphere involves a number of various complicated processes (Text S2). In general, the main conversion processes include:1) the daytime oxidation of NO_2 via OH (OH+NO_2); 2) N_2O_5 uptake on bulk aerosol surfaces at night; 3) nitrate radical (NO_3) reduction via hydrocarbon abstraction (NO_3+HC) at night; 4) the partition of HNO_3 to NO_3^- (Seinfeld and Pandis, 2016). The NO_3+HC and N_2O_5 hydrolysis channels are referred to as nocturnal pathways in the present study. Although few isotopic fractionations during these conversions have been determined in either the field or laboratory, Walters and Michalski (2015a) and Walters et al. (2016) predicted the theoretical N and O isotope equilibrium fractionation factors for conversions between major NOy molecules (NO*x* + HNO_3 + NO_3 + HONO + N_2O_5+ …. +NO_3^-) and O-bearing molecules related to NO*x* oxidation. They did this by using computational quantum chemistry methods. Their pioneering work enabled us to calculate the N/O isotopic fractionation effects of individual conversion pathways, thereby significantly improving our understanding of the atmospheric chemistry of NO*x*. However, how the contribution of pathway-specific contributions to NO_3^- formation can be distinguished and used to determine the NO*x* emission sources in the environment is still up for debate. The three formation pathways are accompanied by distinct N isotopic fractionation effects, and therefore their respective contributions must be addressed accurately for NO*x* source division. However, pathway-specific contributions based solely on O isotopic signatures ($\delta^{18}O$ or $\Delta^{17}O$) may introduce considerable uncertainty (i.e., three pathways, one isotope).

By linking $\delta^{18}O$ and $\delta^{15}N$ of NO_3^- in $PM_{2.5}$ to the oxidation processes, this study investigated the pathway-specific contributions to wintertime NO_3^- in urban Beijing, by determining the $\delta^{18}O$ and $\delta^{15}N$ of NO_3^- in daily $PM_{2.5}$ samples (November 1, 2017 to January 31, 2018). This study had two aims: 1) to reveal the fractional contribution of the three oxidation channels using the $\delta^{18}O$-$\delta^{15}N$ space of NO_3^-; 2) to estimate the nitrogen isotopic signatures of the ambient NO*x* mixture ($\delta^{15}N$-NO*x*) more accurately.

2. Materials and method

2.1. Study site, field sampling, and laboratory analysis

The winter study was carried out in an urban site of the megacity Beijing, at the Chinese Research Academy of Environmental Sciences (40°04′N, 116°42′E); it lasted from November 1, 2017 to January 31, 2018. The sampling site was in a typical urban business and residential region, which has been described in previous studies (Zhang et al., 2020a; Song et al., 2019a, 2019b). The pre-combusted filter for $PM_{2.5}$ sampling (Tissuquartz™ Filters, 2500 QAT-UP, size: 8 × 10 in; Pall Corp., Port Washington, NY, USA) was loaded onto a high-volume air sampler (KC-1000, Laoshan, Qingdao, China), which was set up on the roof of a building (12 m above the ground). The sampler was operated at a flow rate of 1.05 m^3/min for 23.5 h (Zhang et al., 2020a). Once collected, the $PM_{2.5}$ samples were immediately delivered to the laboratory and stored in a fridge. The gaseous HNO_3 and particulate nitrate were likely to have been collected together during the sampling process, and were defined as atmospheric nitrate in this study. A total of 95 samples were collected (92 $PM_{2.5}$ samples, and 3 blanks). Details of the sampling site and procedures have been described elsewhere (Song et al., 2019a, 2019b; Zhang et al., 2020c).

Routine measurements of water-soluble inorganic ions, e.g., NO_3^-, SO_4^{2-} and NH_4^+ were reported in the previous study (Zhang et al., 2020a). In summary, the inorganic ions of interest in the filter samples were extracted ultrasonically using ultrapure water (18.2 MΩ, Millipore) for 30 min. Then, the concentrations of the inorganic ions in the filtered extracts were quantified by ion chromatography (Thermo Fisher Scientific, USA; Zhang et al., 2020c). The limits of detection for the inorganic ions were generally greater than 0.65 μg/L. The reported ionic concentrations of $PM_{2.5}$ samples were recalculated by subtracting those of the blanks. Laboratory analyses of the $\delta^{18}O$ and $\delta^{15}N$ values of the NO_3^- in $PM_{2.5}$ were performed by following a bacterial denitrifier approach (Luo et al., 2019; Sigman et al., 2001; Liu et al., 2018). To summarise, the aqueous NO_3^- in the extract was first converted into gaseous N_2O by the bacteria *Pseudomonas aureofaciens* (with a conversion efficiency higher than 98%), and the produced gaseous N_2O was

then concentrated and fed into a ratio isotopic mass spectrometer (Delta V advantage; Thermo Fisher Scientific, USA) for isotope measurement. International nitrate standards with certified isotopic values (e.g., IAEA-NO_3^-, USGS32, USGS34, USGS35) were used for data calibration. The standards and the $PM_{2.5}$ extracts were adjusted to a final sample size of 20 nmol N. The N/O isotopic values of NO_3^- were also recalculated for each $PM_{2.5}$ sample by using mass balance. The isotopic values of the NO_3^- in $PM_{2.5}$ were reported using the "δ" notation in units per mil (‰):

$$\delta^{15}N - NO_3^- = \left(\frac{\frac{^{15}N}{^{14}N_{sample}}}{\frac{^{15}N}{^{14}N_{N2\ in\ air}}} - 1 \right) \times 1000 \quad (1)$$

$$\delta^{18}N - NO_3^- = \left(\frac{\frac{^{18}O}{^{16}O_{sample}}}{\frac{^{18}O}{^{16}O_{VSMOW}}} - 1 \right) \times 1000 \quad (2)$$

The aerosol properties, i.e., acidity and aerosol liquid water content (ALWC), which have been suggested to significantly affect inorganic nitrate chemistry (i.e., the gas-to-particle exchange), were simulated using the thermodynamic model ISORROPIA-II (Fountoukis and Nenes, 2007; Zhang et al., 2020b). Detailed information on the chemical and thermodynamic model analyses are provided in Text S1.

2.2. End-member mixing of $\delta^{18}O-NO_3^-$ and $\delta^{15}N-NO_3^-$

The $\delta^{18}O-NO_3^-$ signatures can be used to infer the NO_3^- formation channel and are usually elevated when NO*x* is oxidized by O_3. Therefore, a two-endmember linear mixing model was used to assess the respective contribution of daytime and nocturnal pathways, as follows (Phillips and Gregg, 2001):

$$F_{noct} = \frac{\delta^{18}O - NO_{3sample}^- - \delta^{18}O_{day}}{\delta^{18}O_{noct} - \delta^{18}O_{day}} \quad (3)$$

$\delta^{18}O_{day}$ represents the $\delta^{18}O$ endmembers of NO_3^- generated solely via the daytime channel, $\delta^{18}O_{noct}$ represents those generated via nocturnal pathways, and F_{noct} represents the overall fractional contribution of nocturnal pathways to NO_3^- accumulation. For the $\delta^{18}O_{day}$, theoretical values were calculated (≈55‰, Table S1; Fang et al., 2011), while the field $\delta^{18}O_{noct}$ was simulated using the Keeling plot (Pataki et al., 2003; Zhang et al., 2020b):

$$\delta^{18}O - NO_3^-sample = a \cdot \frac{1}{NO_3^-} + b \quad (4)$$

where the intercept of "b" represents the endmembers of $\delta^{18}O_{noct}$ (Table S1).

The overall uncertainty in F_{noct}, taking into account all of the parameters, was calculated as follows:

$$\sigma_F^2 = \frac{1}{(b-a)^2} \left[\sigma_{mix}^2 + (1 - F_{noct})^2 \cdot \sigma_a^2 + F_{noct}^2 \cdot \sigma_b^2 \right] \quad (5)$$

with "mix", "a", and "b" representing $\delta^{18}O-NO_3^-$sample, $\delta^{18}O_{day}$, and $\delta^{18}O_{noct}$ for brevity, respectively. Usually, the overall uncertainty was in the order of 5% for F_{noct}, with the denominator as high as 50‰ in the present study (Table S1).

In theory, $\delta^{18}O-NO_3^-$ should have been significantly and positively correlated with $\delta^{15}N-NO_3^-$ during haze development, when the N_2O_5 channel dominated the nitrate accumulations (Fig. 1B). Otherwise, $\delta^{18}O-NO_3^-$ should have been negatively correlated with $\delta^{15}N-NO_3^-$, when the NO_3+HC channel surpassed the N_2O_5 channel in NO_3^- formation. Furthermore, the $\delta^{15}N$ endmembers of NO_3^- from daytime and nocturnal pathways ($\delta^{15}N_{day}$ and $\delta^{15}N_{noct}$, respectively) were inferred using their respective $\delta^{18}O-NO_3^-$ endmembers and the correlations of $\delta^{18}O-NO_3^-$ with $\delta^{15}N-NO_3^-$ in the $PM_{2.5}$ samples (Fig. 1A and B). More importantly, the $\delta^{15}N_{noct}$ endmembers were determined by the relative prevalence of the NO_3+HC channel or the N_2O_5 channel in the overall nocturnal NO_3^- formation. Therefore, the slopes of $\delta^{18}O-NO_3^-$ against $\delta^{15}N-NO_3^-$ reflected their relative fractional contributions. The difference between $\delta^{15}N_{day}$ and $\delta^{15}N_{noct}$ (Δ_N in Fig. 1A) represents the absolute difference of nitrogen isotopic fractionation factors from NO*x* to NO_3^- between the field daytime and nocturnal channels (as εN_{day} and εN_{noct}, respectively, Fig. 1A).

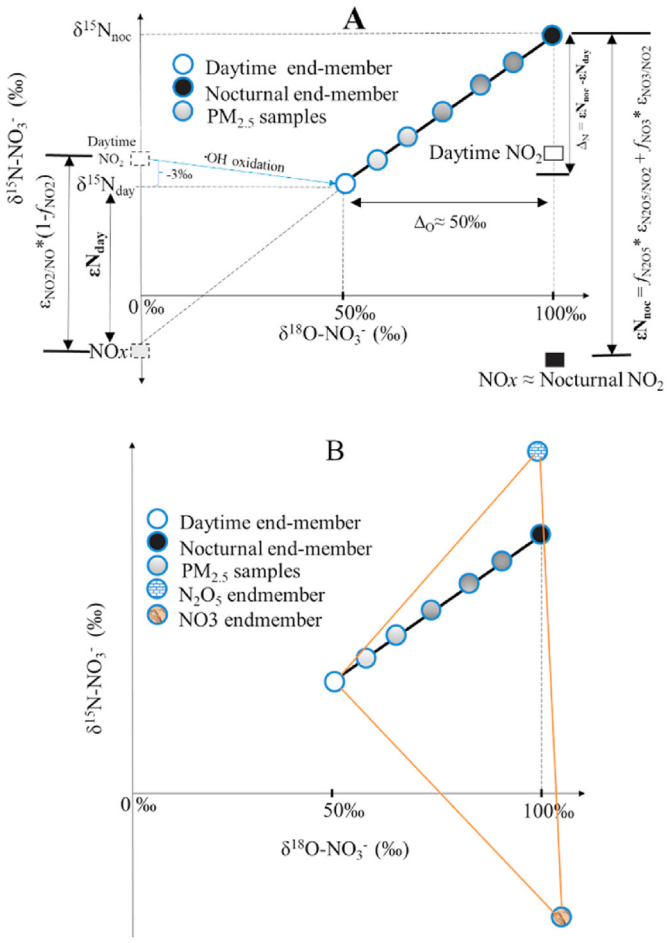

Fig. 1. Correlations between $\delta^{15}N-NO_3^-$ and $\delta^{18}O-NO_3^-$ of $PM_{2.5}$ samples (A and B). Panel A shows the N isotopic fractionation effects of individual processes during the conversion of NO*x* to NO_3^-. εN_{day} represented the overall N isotopic fractionation effects of daytime pathways converting NOx to NO_3^-; while εN_{noct} represented those through nocturnal pathways. Δ_N represented the difference of $\delta^{15}N$ endmembers between daytime and nocturnal channels ($\delta^{15}N_{day}$ and $\delta^{15}N_{noct}$, respectively), and also the difference between εN_{day} and εN_{noct}. Panel B shows the slope of $\delta^{15}N-NO_3^-$ against $\delta^{18}O-NO_3^-$ for field $PM_{2.5}$ samples determined by the relative contribution of N_2O_5 and NO_3 channels to the overall nocturnal pathway. Detailed interpretations were provided in the main text and supporting information.

2.3. Pathway-specific contributions to NO_3^- in $PM_{2.5}$: insights from regressions of $\delta^{18}O-NO_3^-$ versus $\delta^{15}N-NO_3^-$

Initially, we estimated the relative contribution of daytime and nocturnal pathways to NO_3^- in $PM_{2.5}$ by using Eqns (1)-3), and thereby the respective contributions of N_2O_5 and NO_3+HC pathways (F_{N2O5} and F_{NO3}, respectively) were quantified based on the absolute difference between the field εN_{noct} (determined by the relative importance of the NO_3+HC and N_2O_5 channels) and the theoretical εN_{N2O5} (Fig. 1B, Eqn S6 in Text S2). As aforementioned, the slope of $\delta^{18}O-NO_3^-$ against $\delta^{15}N-NO_3^-$ is determined by the respective contributions of the N_2O_5 and NO_3+HC pathways, and therefore, can be used to calculate the difference between field εN_{noct} and theoretical εN_{N2O5}. Overall, by linking the $\delta^{15}N-NO_3^-$ to the NO*x* oxidation chemistry, our new isotopic perspective provides another way to assess the fractional contributions of specific pathways to NO_3^- in $PM_{2.5}$. The corresponding uncertainties in the calculations of these parameters were provided in Text S3.

2.4. Simulation of the $\delta^{15}N$ signatures of in-situ NOx

In this study, we were interested in both the daily δ^{15}N-NO*x* (δ^{15}N signatures of *in-situ* NO*x*) and monthly mean values of δ^{15}N-NO*x*, which can be calculated using the following independent approaches.

A) Monthly mean values of δ^{15}N-NO*x*; inferred from the differences between the $\delta^{15}N_{day}$ and isotopic fractionation factor of the daytime pathways (εN_{day}), or from the differences between the $\delta^{15}N_{noct}$ and isotopic fractionation factor of the nocturnal pathways (εN_{noct}), for which εN_{noct} was approximated to εN_{day} plus 8.5‰ (Fig. 1A).

B) Daily δ^{15}N-NO*x*; the overall isotopic fractionation factors (εN) from NO*x* to NO_3^- can be estimated by considering the individual εN values of the specific pathways (Text S2) with respect to their relative fractional contributions (Eqn. (4)), so the δ^{15}N-NO*x* was formulated as:

$$\varepsilon N = (1 - F_{noct}) \cdot \varepsilon_{Nday} + F_{N2O5} \cdot \varepsilon N_{N2O5} + F_{NO3} \cdot \varepsilon N_{NO3} \quad (6)$$

$$\delta^{15}\text{N-NO}x = \delta^{15}\text{N}-NO_3^-{}_{sample} - \varepsilon N \quad (7)$$

The individual (i.e., εN_{day}, εN_{N2O5}, εN_{NO3}) and overall uncertainties of εN, taking the propagation of uncertainty of each factor (Eqn. (4)) into account, were greater than 5‰ (Text S3).

3. Results and discussion

3.1. Overview of the observations

Major inorganic ions in the 23.5-h integrated $PM_{2.5}$ samples (e.g., SO_4^{2-}, NO_3^-, NH_4^+), the aerosol properties (i.e., pH and ALWC), and the meteorological conditions during the sampling period are presented in Fig. 2. As is consistent with previous studies, the periodic cycle of haze episodes was usually in the order of 4–7 days (Fu et al., 2020; Guo et al., 2014). In general, the temporal evolution of aerosol inorganic chemical species, aerosol acidity, water content, and even the $\delta^{18}O-NO_3^-$ and $\delta^{15}N-NO_3^-$ values were related to the occurrence of haze pollution. Specifically, the above-mentioned proxies increased rapidly from clean days to haze episodes, except for the O_3 (Fig. 2, Fig.S2). As the most abundant secondary inorganic chemical species, the mean concentration of NO_3^- was 8.74 μg/m^3 (from 0.66 to 43.52 μg/m^3), higher than that of SO_4^{2-} (mean of 4.36 μg/m^3, from 0.50 to 27.51 μg/m^3). The ratio of NO_3^-/SO_4^{2-} increased from 0.3 during clean days to 3.1 in haze episodes, suggesting an enhanced NO_3^- formation potential, and highlighting the importance of NO_3^- in fine aerosol development. The dominance of NO_3^- over SO_4^{2-} in mass during haze pollution in the North China Plain (NCP) region has been reported previously and was mainly attributed to the emission mitigation efforts in recent years (Fu et al., 2020; Xu et al., 2019; Zhao et al., 2019). During the campaign, the aerosol pH inferred from the thermodynamic analysis was 5.4 on average, ranging from 2.5 to 6.6 (Fig. 1), which was in-line with previous reports (Ding et al., 2019; K. Li et al., 2019). The simulated ALWC ranged from 5 μg/m^3 to 230 μg/m^3, which was comparable to the corresponding $PM_{2.5}$ concentrations (Fig. 2). Such high aerosol pH and ALWC values have been reported previously across the NCP region, and were regarded as a distinct feature of the particulate matter in that region when compared to those of the United States and Europe (Guo et al., 2015; Shi et al., 2017; Song et al., 2018, 2019a, 2019b). Higher pH and ALWC values facilitate the

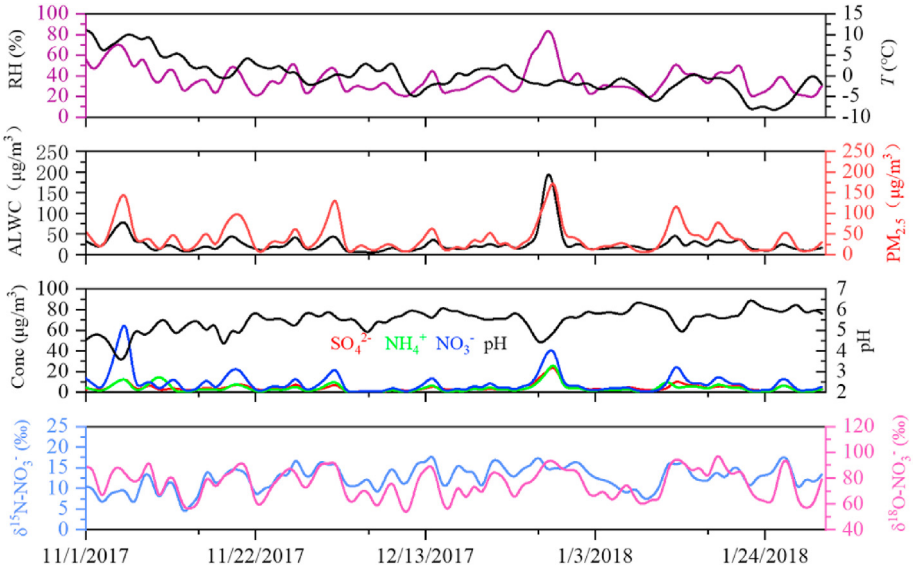

Fig. 2. Time series of meteorological variables (i.e., RH, T), aerosol properties (pH, ALWC), mass concentrations of $PM_{2.5}$, and major ions (NH_4^+, NO_3^- and SO_4^{2-}) in the winter of 2017–2018 (1 November-31 January).

gas-particle partitioning of atmospheric nitrate, which leads to more than 95% of the atmospheric nitrate partitioned into the particle phase in this study (Fig.S1, Ding et al., 2019; Liu et al., 2017; Song et al., 2019a, 2019b). Therefore, the N isotopic fractionation effect between gaseous HNO_3 and particulate NO_3^- may be minor and was not considered in this study.

The $\delta^{15}N{-}NO_3^-$ ranged widely from +2.8‰ to +19.6‰, with a mean of +12.9‰ ± 3.5‰ during the sampling period (Fig. 2). In general, the averaged $\delta^{15}N{-}NO_3^-$ values of the $PM_{2.5}$ in winter 2017–2018 were comparable to those reported previously in urban Beijing. For example, $\delta^{15}N{-}NO_3^-$ values of $PM_{2.5}$ ranged from −2.3‰ to +19.7‰ (+11.9‰ ± 4.4‰) in the winter of 2014 (Song et al., 2019a, 2019b), −2.5‰ to +19.2‰ (approximately +12.3‰) from October 2014 to January 2015 (He et al., 2018), and +1.3‰ to +21.2‰ (+13.0‰ ± 4.7‰) from February to April 2013 (Luo et al., 2019). Comparing the $\delta^{15}N{-}NO_3^-$ values directly among different years and sampling sites was not recommended. This is because the determined $\delta^{15}N{-}NO_3^-$ value is a complex function of the combined initial nitrogen isotopic signatures of various NO*x* sources and any given nitrogen isotopic fractionation effect during NO*x* conversions. However, the small variations of wintertime-averaged $\delta^{15}N{-}NO_3^-$ values since 2013 were surprising, given that the ^{15}N-enriched NO*x* emitted from coal combustion or heavy-duty diesel-powered trucks was cut or replaced by the relatively ^{15}N-depleted NO*x* from natural gas (+14.5 ± 4.4‰ *vs* −16.5 ± 1.7‰, respectively, Walters et al., 2015a; Walters et al., 2015b; Zhang et al., 2020c). Combined with the reported NO*x* emission inventory (Fig. S3), one of the more likely explanations for these results is that the transportation sector was the dominant NO*x* emission source in the urban environment.

The $\delta^{18}O{-}NO_3^-$ (mean of +74.9‰ ± 13.4‰) also varied widely, from +55.3‰ to +103.5‰ during the observations. In general, the determined $\delta^{18}O{-}NO_3^-$ falls within the broad ranges given in previous reports for $PM_{2.5}$ or precipitation (e.g., +49.4‰ to +103.9‰, see Zong et al., 2017; Luo et al., 2019, Song et al., 2019a, 2019b, and references therein). However, the mean $\delta^{18}O{-}NO_3^-$ value in the current study (winter 2017–2018) seemed lower than in the above-mentioned reports; there it was generally higher than +80‰ (Luo et al., 2019; Song et al., 2019a, 2019b; Zong et al., 2020; Zhang et al., 2020a). Usually, the $\delta^{18}O{-}NO_3^-$ was highly dependent on its formation pathways, elevating proportionally with the nocturnal pathways dominant in the conversion of NOx to NO_3^-. For example, the $\delta^{18}O{-}NO_3^-$ showed a strong positive correlation with the NO_3^- concentrations during the sampling period (Fig. S5). This implied that the nocturnal pathways played an important role in high NO_3^- concentrations during winter in Beijing. Therefore, the declined wintertime $\delta^{18}O{-}NO_3^-$ from 2013 to 2017 may be attributed to increased photochemistry activity, which facilitated the chemical conversion of NO*x* to NO_3^- (Fu et al., 2020; Lu et al., 2019; Womack et al., 2019). For instance, the estimated contribution of the OH oxidation channel to the overall NO_3^- concentrations averaged 45.3% during the sampling period (see Section 3.3), which was higher than that reported in previous studies. Furthermore, an extremely high mixing ratio and turnover rate of OH ($1–8 \times 10^6$ cm^{-3}) was reported in Beijing in the winter of 2016. This was based on direct field observations, which were comparable with those determined in the summer study (Lu et al., 2019). The observed ^{18}O-depleted NO_3^- in this study could mainly be due to the elevated proportion of wintertime photochemical pathways.

3.2. *Correlations between daily $\delta^{18}O{-}NO_3^-$ versus $\delta^{15}N{-}NO_3^-$*

The daily field $\delta^{18}O{-}NO_3^-$ was significantly and linearly correlated with the corresponding $\delta^{15}N{-}NO_3^-$ throughout the winter, with extremely similar slopes observed for the three months (slopes = 0.171–0.179, Fig. 3), and the intercept varying

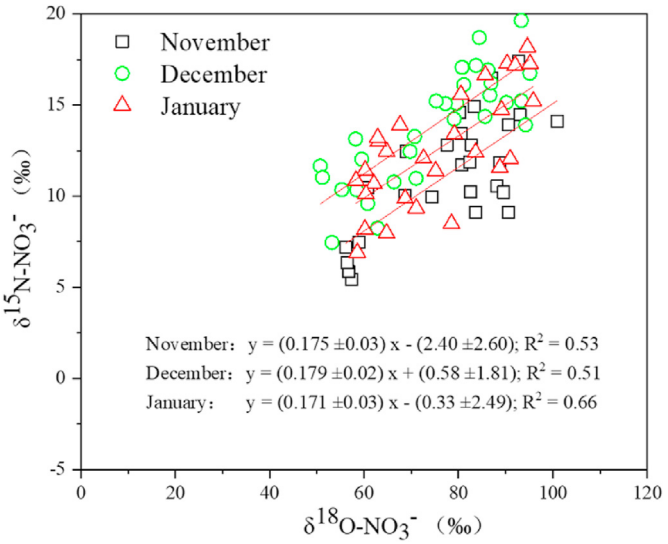

Fig. 3. Relationships between $\delta^{15}N{-}NO_3^-$ and $\delta^{18}O{-}NO_3^-$. November: black square; December: green circle; January: red triangle. The underlined environmental significance was presented in Fig. 1 and the main text. (For interpretation of the references to colour in this figure legend, the reader is referred to the Web version of this article.)

from −2.4 ± 2.6 to 0.58 ± 1.8. The points deviating from linear regressions can be attributed to: 1) fluctuation of source NO*x*; 2) variation of f_{NO2} and temperature; 3) Rayleigh fractionations during the rapid buildup of NO_3^-; and, 4) the possible influence of aerosol deposition. At a first glance, the regression slope seemed to be driven by the relative difference in $\delta^{18}O$-$\delta^{15}N$ endmembers between daytime and nocturnal channels, with the means of $\delta^{15}N$ (Δ_N) and $\delta^{18}O$ differences estimated to be approximately 8.5‰ and 40‰, respectively (Fig. 1A). In fact, the regression slope was determined by the relative contributions of the N_2O_5 hydrolysis and NO_3+HC formation pathways within a specific period (Fig. 1B), as the two channels were characterized by similar $\delta^{18}O$ endmembers but distinct $\delta^{15}N$ endmembers (Fig. 1B, Table S1). This implied that the field $\delta^{15}N{-}NO_3^-$ was directly linked to the oxidation chemistry of NO*x*. Under typical wintertime meteorological conditions in Beijing (mean temperature of 273.25 K, temperatures ranging from 264.85 K to 277.25 K), the $\delta^{15}N_{N2O5}$ and $\delta^{15}N_{NO3}$ were calculated to be approximately +29.8‰ (from +28.8‰ to +31.0‰) and −19.1‰ (from −19.4‰ to −18.8‰), while the field $\delta^{15}N_{noct}$ was approximated to +21.4‰ ($\varepsilon N_{day}+\Delta_N$), assuming $\delta^{15}N\text{-}NOx$ = 0‰ (also nocturnal $\delta^{15}N{-}NO_2$ = 0‰). Therefore, the linear regressions offered a new way to distinguish the contribution of the N_2O_5 hydrolysis and NO_3+HC channels relative to the overall nocturnal pathways (Fig. 1 and see below for more discussion).

3.3. *Estimates of the fractional contributions of specific pathways based on the $\delta^{18}O$-$\delta^{15}N$ space of NO_3^-*

The estimated $\delta^{18}O_{noct}$ endmembers varied from +92.5‰ to +98.9‰ (intercept of regressions in Fig. 4) during the sampling period. Notably, the mean value (+95.2‰) compared well with that estimated by using the theoretical approach (Table S1; Walters et al., 2016). The daily $\delta^{18}O{-}NO_3^-$ exhibited large variability (from +55.3‰ to +103.5‰), yet was significantly and positively correlated with the NO_3^- concentrations, implying a role of O_3 oxidation in the buildup of atmospheric NO_3^- (Fig. S5). Due to the large denominator in Eqn. (3), the overall uncertainty of the nocturnal pathway contribution was in the order of 5%. The daily contributions of the nocturnal channels declined with time (Fig.S6;

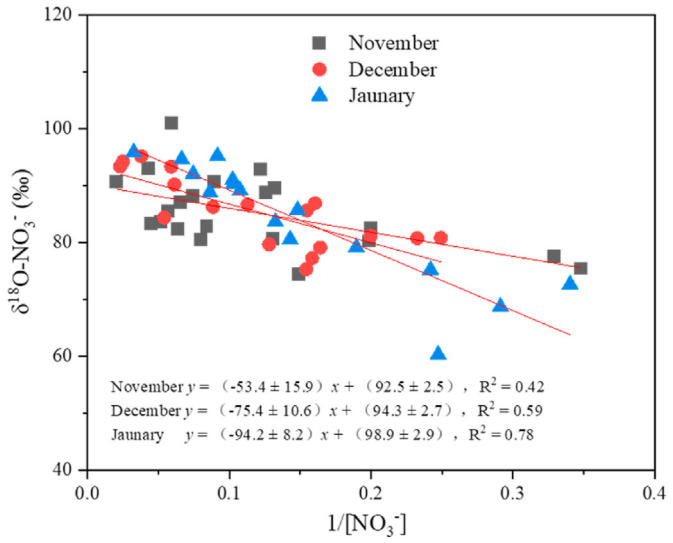

Fig. 4. Keeling plots of $\delta^{18}O-NO_3^-$ against $1/NO_3^-$. November $PM_{2.5}$ samples are shown with black squares, December with red circles, and January with blue triangles. The intercept represented the $\delta^{18}O$ endmembers of NO_3^- generated via nocturnal pathways.

Table S2), and the monthly mean values were 62.1%, 53.5%, and 45.8% for November, December, and January, respectively. On average, approximately 54.7% of the NO_3^- in the $PM_{2.5}$ was generated from the nocturnal pathways during the winter sample period.

Linking the $\delta^{15}N-NO_3^-$ to the NO*x* oxidation chemistry, our new strategy suggested that the N_2O_5 channel contributed approximately 85 ± 2% relative to the other nocturnal pathways. This was comparable across the three months due to the similarity of the regression slopes of $\delta^{18}O-NO_3^-$ against $\delta^{15}N-NO_3^-$ (Figs. 1 and 3). Overall, the relative fractional contributions (mean ± sd) of the $OH+NO_2$, N_2O_5, and NO_3+HC channels to the atmospheric NO_3^- were estimated to be 45.3 ± 30.2%, 46.5 ± 25.6%, and 8.2 ± 4.5%, respectively, in the winter of 2017–2018 in urban Beijing (Table 1). The relatively large standard errors associated with the individual channels can be attributed to the distinct wintertime atmospheric chemical conditions seen day-to-day during the sampling period (Fig. 2, Fig.S3). In general, our estimates were consistent with previous reports conducted in urban Beijing based on either $\Delta^{17}O-NO_3^-$ or $\delta^{18}O-NO_3^-$, suggesting that nocturnal pathways dominated NO_3^- accumulation in the winter (Fan et al., 2020; Song et al., 2020; Wang et al., 2019; He et al., 2017). However, the presented estimates significantly differed from the corresponding values estimated using $\Delta^{17}O-NO_3^-$ in the winter of 2013–2014 and 2015 in urban Beijing ($OH+NO_2$ = 31 ± 11%, N_2O_5 ≈ 35 ± 17%, and NO_3+HC ≈ 34 ± 12%), due to the significant differences in the estimated proportional contribution of the NO_3+HC pathway (Wang et al., 2019; Song et al., 2020). The NO_3+HC pathway should be less important in nitrate accumulation. For example, a recent global modelling study suggested that nitrate production from the NO_3+HC pathway only accounted for 4–5% of the annual global surface nitrate production on average, while OH oxidation was as important as N_2O_5 uptake globally (both 41%, Alexander et al., 2020). Moreover, the NO_3+HC pathway was estimated to contribute 1–10% of the atmospheric NO_3^- during an annual study in La Jolla, USA (Michalski et al., 2003). The potential of $\delta^{15}N-NO_3^-$ for use in evaluating NO*x* oxidation chemistry has been suggested previously (Walters and Michalski, 2016), yet the current study was one of few that have utilized $\delta^{15}N-NO_3^-$ in the assessment of pathway-specific contributions.

3.4. $\delta^{15}N$ signatures of atmospheric NOx and the potential NOx emission sources during winter in Beijing

The overall εN values from NO*x* to NO_3^- were estimated to be on average + 16.3 ± 1.8‰ (ranging from +13.2‰ to +19.5‰, Fig. S7), resembling those estimated based on the $\Delta^{17}O-NO_3^-$ approach (+15.8 ± 7.4‰) in January 2015 in Beijing (Song et al., 2020). Generally, the uncertainty of daily εN from NO*x* to NO_3^- was roughly 5‰ (Text S4). Moreover, the $\delta^{15}N$ signatures of the monthly mixtures of NO*x* simulated by the two independent approaches were comparable (Table 1). The mean monthly $\delta^{15}N$ signatures of ambient NO*x* based on approach A were −5.9‰, −3.8‰, and −3.6‰ for November, December, and January, respectively; these were close to the corresponding monthly mean values based on approach B (−5.5‰, −2.7‰, and −3.2‰, respectively). The overall uncertainties in the ambient $\delta^{15}N$-NO*x* based on approaches A and B were 5.2‰ and 5‰, respectively, implying that our simple strategies for the estimation of pathway-specific contributions and nitrogen isotopic fractionation effects based on the $\delta^{18}O$-$\delta^{15}N$ space of NO_3^- were robust. One of the great advantages of the current approach was the absence of numerous assumptions, potentially reducing the uncertainties of the estimated εN and $\delta^{15}N$ values in the ambient mixture of NO*x*.

The monthly $\delta^{15}N$-NO*x* signatures were within the range of the NO*x* emitted from vehicular exhaust (−3.7 ± 10.4‰, Walters et al., 2015a; Walters et al., 2015b; Zong et al., 2017), indicating that transportation was a major contributor to ambient NO_3^- in the $PM_{2.5}$ preliminary. Based on multiple isotopic evidence ($\Delta^{14}C$, $\delta^{13}C$, $\delta^{15}N-NH_4^+$, and $\delta^{15}N-NO_3^-$), Lim et al. (2020) also suggested that liquid fossil fuel combustion, especially vehicle exhaust, significantly enhanced the accumulation of secondary inorganic aerosols in urban Beijing in the spring of 2016. The dominance of NO*x* emitted from the transport sector can also account for the minor variations in wintertime-averaged $\delta^{15}N-NO_3^-$ values in recent winter seasons in urban Beijing. Furthermore, Beijing's local emission inventory (e.g., MEIC) also indicated that transportation was the key contributor to NO*x* emissions in 2017 (approximately 75%, Fig. S3). Together, these results indicated that vehicle emissions were the key contributing source to NO*x* in the megacity of Beijing in recent years.

Table 1
The calculated contribution of the individual oxidation pathway (F_{OH}: contribution of OH oxidation channel, F_{N2O5}: N_2O_5 hydrolysis channel, F_{NO3}: NO_3 reacted with hydrocarbon), the nitrogen isotopic fractionation factor from NO*x* to NO_3^- (εN), and the estimated source signatures of NO*x* ($\delta^{15}N$-NO*x*) during the sampling period.

	F_{OH}	F_{N2O5}	F_{NO3}	εN	$\delta^{15}N$-NO*x* (A)	$\delta^{15}N$-NO*x* (B)
November	37.8 ± 30.1%[a]	52.8 ± 25.6%[a]	9.3 ± 4.5%[a]	16.5 ± 1.6‰	−5.9‰	−5.5 ± 2.6‰
December	47.1 ± 30.9%[a]	44.9 ± 26.2%[a]	7.9 ± 4.6%[a]	16.5 ± 1.8‰	−3.8‰	−2.7 ± 1.9‰
January	51.6 ± 28.1%[a]	41.0 ± 23.9%[a]	7.2 ± 4.2%[a]	15.8 ± 2.0‰	−3.6‰	−3.2 ± 2.2‰
Mean	45.3 ± 30.2%	46.5 ± 25.6%	8.2 ± 4.5%	16.3 ± 1.8‰	−4.4 ± 1.2‰	−3.8 ± 2.5‰

The uncertainty associated with each parameter is included in Text S3. Categories that share common letters do not differ significantly ($p > 0.05$). $\delta^{15}N$-NO*x* (A) and $\delta^{15}N$-NO*x* (B) represented the initial NOx signatures derived from two independent approaches (see material and method 2.4).

4. Conclusions

Particulate nitrate is playing an increasingly important role in haze development during winter, making the reduction of NO*x* emission a top priority for further $PM_{2.5}$ pollution mitigation. However, the emission inventory of NO*x* remains highly controversial. Our improved isotopic approach highlighted that the transport sector was the largest emitter in the winter of 2017 in Beijing. Combined with previous reports on $\delta^{15}N{-}NO_3^-$ in $PM_{2.5}$, we also inferred that vehicles were the major contributors to NO*x* emissions between 2013 and 2017 in Beijing. The results of the NO*x* source divisions were in-line with the published regional emission inventories from the MEIC models. Therefore, our results revealed that control measures on transportation should be implemented for continued air quality improvement. More research should be conducted in other city clusters to further explain the NO*x* emission inventory regionally, by using the approved source apportionment methods. For the megacity of Beijing, the NO*x* concentration was estimated to have declined by 20% between 2013 and 2017, whereas the particulate nitrate fraction increased during this period. The increasing role of nitrate aerosol in haze pollution was driven by the high conversion efficiency of NO*x* to NO_3^-, resulting from increased atmospheric oxidant concentrations (i.e., O_3 and $\cdot OH$) and the abundance of alkaline gas, NH_3. Previous pollution mitigation policies have concentrated on cutting emissions of nitrate aerosol precursors of NO*x*. However, the atmospheric reactions involving NO*x* and radicals/oxidants (e.g., OH and O_3) are complex, leading to a non-linear response in regional haze pollution as a result of efforts to mitigate NOx emissions. Overall, concurrent reductions of NO*x*, NH_3, and VOCs (volatile organic compounds) are necessary to further improve clean air policies.

Author contributions

Zhongyi Zhang: Conceptualization, Software, Investigation, Writing – original draft. Hui Guan: Conceptualization, Software, Investigation, Writing – original draft. Li Luo: Methodology, Resources, Writing – review & editing, Data curation: Resources, Writing – review & editing, Data curation. Cheng Liu, Yue Liang, Hongwei Xiao and Xiaozhen Fang: Resources, Writing – review & editing. Huayun Xiao: Funding acquisition; Project administration; Supervision; Validation; Writing – review & editing.

Declaration of competing interest

The authors declare that they have no conflicts of interest.

Acknowledgments

This work was supported by the National Natural Science Foundation of China (Grant no. 41863001 and 41425014), the Key Laboratory Project of Jiangxi Province (20171BCD40010) and the Two 1000 Talents Plan Project of Jiangxi Province (S2018CQKJ0755). Data used in this paper are available upon request from the corresponding author (xiaohuayun@ecut.edu.cn).

Appendix A. Supplementary data

Supplementary data to this article can be found online at https://doi.org/10.1016/j.envpol.2021.116708.

References

Alexander, B., Sherwen, T., Holmes, C., Fisher, J., Chen, Q., Evans, M., Kasibhatla, P., 2020. Global inorganic nitrate production mechanisms: comparison of a global model with nitrate isotope observations. Atmos. Chem. Phys. Discuss. 1–36.
An, Z., Huang, R.-J., Zhang, R., Tie, X., Li, G., Cao, J., Zhou, W., Shi, Z., Han, Y., Gu, Z., Ji, Y., 2019. Severe haze in northern China: a synergy of anthropogenic emissions and atmospheric processes. Proc. Natl. Acad. Sci. U.S.A. 116, 8657–8666.
Chang, Y., Zhang, Y.-L., Li, J., Tian, C., Song, L., Zhai, X., Zhang, W., Huang, T., Lin, Y.-C., Zhu, C., Fang, Y., Lehmann, M.F., Chen, J., 2019. Isotopic constraints on the atmospheric sources and formation of nitrogenous species in clouds influenced by biomass burning. Atmos. Chem. Phys. 19, 12221–12234.
Cheng, J., Su, J., Cui, T., Li, X., Dong, X., Sun, F., Yang, Y., Tong, D., Zheng, Y., Li, Y., 2019. Dominant role of emission reduction in $PM_{2.5}$ air quality improvement in Beijing during 2013–2017: a model-based decomposition analysis. Atmos. Chem. Phys. 19, 6125–6146.
Ding, J., Zhao, P., Su, J., Dong, Q., Du, X., Zhang, Y., 2019. Aerosol pH and its driving factors in Beijing. Atmos. Chem. Phys. 19, 7939–7954.
Elliott, E.M., Yu, Z., Cole, A.S., Coughlin, J.G., 2019. Isotopic advances in understanding reactive nitrogen deposition and atmospheric processing. Sci. Total Environ. 662, 393–403.
Fan, M.Y., Zhang, Y.L., Lin, Y.C., Cao, F., Zhao, Z.Y., Sun, Y., Qiu, Y., Fu, P., Wang, Y., 2020. Changes of emission sources to nitrate aerosols in Beijing after the clean air actions: evidence from dual isotope compositions. J. Geophys. Res. Atmos. 125, e2019JD031998.
Fang, Y., Koba, K., Wang, X., Wen, D., Li, J., Takebayashi, Y., Liu, X., Yoh, M., 2011. Anthropogenic imprints on nitrogen and oxygen isotopic composition of precipitation nitrate in a nitrogen-polluted city in southern China. Atmos. Chem. Phys. 11, 1313.
Fountoukis, C., Nenes, A., 2007. Isorropia II: a computationally efficient thermodynamic equilibrium model for $K^+{-}Ca^{2+}{-}Mg^{2+}{-}NH_4^+{-}Na^+{-}SO_4^{2-}{-}NO_3^-{-}Cl^-{-}H_2O$ aerosols. Atmos. Chem. Phys. 7, 4639–4659.
Fu, X., Wang, T., Gao, J., Wang, P., Liu, Y., Wang, S., Zhao, B., Xue, L., 2020. Persistent heavy winter nitrate pollution driven by increased photochemical oxidants in northern China. Environ. Sci. Technol.
Guo, S., Hu, M., Zamora, M.L., Peng, J., Shang, D., Zheng, J., Du, Z., Wu, Z., Shao, M., Zeng, L., Molina, M.J., Zhang, R., 2014. Elucidating severe urban haze formation in China. Proc. Natl. Acad. Sci. U.S.A. 111, 17373–17378.
Guo, H., Xu, L., Bougiatioti, A., Cerully, K.M., Capps, S.L., Hite, J.R., Carlton, A.G., Lee, S.H., Bergin, M.H., Ng, N.L., Nenes, A., Weber, R.J., 2015. Fine-particle water and pH in the southeastern United States. Atmos. Chem. Phys. 15, 5211–5228.
He, P., Xie, Z., Chi, X., Yu, X., Fan, S., Kang, H., Liu, C., Zhan, H., 2018. Atmospheric $\Delta^{17}O(NO_3^-)$ reveals nocturnal chemistry dominates nitrate production in Beijing haze. Atmos. Chem. Phys. 18, 14465–14476.
Huang, R.-J., Zhang, Y., Bozzetti, C., Ho, K.-F., Cao, J.-J., Han, Y., Daellenbach, K.R., Slowik, J.G., Platt, S.M., Canonaco, F., 2014. High secondary aerosol contribution to particulate pollution during haze events in China. Nature 514 (7521), 218–222.
Li, M., Liu, H., Geng, G., Hong, C., Liu, F., Song, Y., Tong, D., Zheng, B., Cui, H., Man, H., 2017. Anthropogenic emission inventories in China: a review. Natl. Sci. Rev. 4, 834–866.
Li, H., Cheng, J., Zhang, Q., Zheng, B., Zhang, Y., Zheng, G., He, K., 2019. Rapid transition in winter aerosol composition in Beijing from 2014 to 2017: response to clean air actions. Atmos. Chem. Phys. 19, 11485–11499.
Li, K., Jacob, D.J., Liao, H., Shen, L., Zhang, Q., Bates, K.H., 2019. Anthropogenic drivers of 2013-2017 trends in summer surface ozone in China. Proc. Natl. Acad. Sci. U. S. A 116, 422–427.
Lim, S., Yang, X., Lee, M., Li, G., Gao, Y., Shang, X., Zhang, K., Czimczik, C.I., Xu, X., Bae, M.S., Moon, K.J., Jeon, K., 2020. Fossil-driven secondary inorganic $PM_{2.5}$ enhancement in the North China Plain: evidence from carbon and nitrogen isotopes. Environ. Pollut. 266, 115163.
Liu, M., Song, Y., Zhou, T., Xu, Z., Yan, C., Zheng, M., Wu, Z., Hu, M., Wu, Y., Zhu, T., 2017. Fine particle pH during severe haze episodes in northern China. Geophys. Res. Lett. 44, 5213–5221.
Liu, X.-Y., Koba, K., Koyama, L.A., Hobbie, S.E., Weiss, M.S., Inagaki, Y., Shaver, G.R., Giblin, A.E., Hobara, S., Nadelhoffer, K., 2018. Nitrate is an important nitrogen source for Arctic tundra plants. Proc. Natl. Acad. Sci. U.S.A. 115, 3398–3403.
Liu, X.-Y., Yin, Y.-M., Song, W., 2020. Nitrogen isotope differences between major atmospheric NOy species: implications for transformation and deposition processes. Environ. Sci. Technol. Lett. 7, 227–233.
Lu, K., Fuchs, H., Hofzumahaus, A., Tan, Z., Wang, H., Zhang, L., Schmitt, S.H., Rohrer, F., Bohn, B., Broch, S., 2019. Fast photochemistry in wintertime haze: consequences for pollution mitigation strategies. Environ. Sci. Technol. 53, 10676–10684.
Luo, L., Wu, Y., Xiao, H., Zhang, R., Lin, H., Zhang, X., Kao, S.-j., 2019. Origins of aerosol nitrate in Beijing during late winter through spring. Sci. Total Environ. 653, 776–782.
Michalski, G., Scott, Z., Kabiling, M., Thiemens, M.H., 2003. First measurements and modeling of $\Delta^{17}O$ in atmospheric nitrate. Geophys. Res. Lett. 30, 1870.
Pataki, D.E., Ehleringer, J.R., Flanagan, L.B., Yakir, D., Bowling, D.R., Still, C.J., Buchmann, N., Kaplan, J.O., Berry, J.A., 2003. The application and interpretation of Keeling plots in terrestrial carbon cycle research. Global Biogeochem. Cycles 17.
Phillips, D.L., Gregg, J.W., 2001. Uncertainty in source partitioning using stable isotopes. Oecologia 127, 171–179.
Seinfeld, J.H., Pandis, S.N., 2016. Atmospheric Chemistry and Physics: from Air Pollution to Climate Change. John Wiley & Sons.
Shi, G., Xu, J., Peng, X., Xiao, Z., Chen, K., Tian, Y., Guan, X., Feng, Y., Yu, H., Nenes, A.,

Russell, A.G., 2017. pH of aerosols in a polluted atmosphere: source contributions to highly acidic aerosol. Environ. Sci. Technol. 51, 4289–4296.
Sigman, D.M., Casciotti, K.L., Andreani, M., Barford, C., Galanter, M., Böhlke, J., 2001. A bacterial method for the nitrogen isotopic analysis of nitrate in seawater and freshwater. Anal. Chem. 73, 4145–4153.
Song, S., Gao, M., Xu, W., Shao, J., Shi, G., Wang, S., Wang, Y., Sun, Y., McElroy, M.B., 2018. Fine-particle pH for Beijing winter haze as inferred from different thermodynamic equilibrium models. Atmos. Chem. Phys. 18, 7423–7438.
Song, S., Nenes, A., Gao, M., Zhang, Y., Liu, P., Shao, J., Ye, D., Xu, W., Lei, L., Sun, Y., 2019a. Thermodynamic modeling suggests declines in water uptake and acidity of inorganic aerosols in beijing winter haze events during 2014/2015–2018/2019. Environ. Sci. Technol. Lett. 6 (12), 752–760.
Song, W., Wang, Y.-L., Yang, W., Sun, X.-C., Tong, Y.-D., Wang, X.-M., Liu, C.-Q., Bai, Z.-P., Liu, X.-Y., 2019b. Isotopic evaluation on relative contributions of major NOx sources to nitrate of $PM_{2.5}$ in Beijing. Environ. Pollut. 248, 183–190.
Song, W., Liu, X.-Y., Wang, Y.-L., Tong, Y.-D., Bai, Z.-P., Liu, C.-Q., 2020. Nitrogen isotope differences between atmospheric nitrate and corresponding nitrogen oxides: a new constraint using oxygen isotopes. Sci. Total Environ. 701, 134515.
Sun, Y., Lei, L., Zhou, W., Chen, C., He, Y., Sun, J., Li, Z., Xu, W., Wang, Q., Ji, D., Fu, P., Wang, Z., Worsnop, D.R., 2020. A chemical cocktail during the COVID-19 outbreak in Beijing, China: insights from six-year aerosol particle composition measurements during the Chinese New Year holiday. Sci. Total Environ. 742, 140739.
Walters, W.W., Michalski, G., 2015. Theoretical calculation of nitrogen isotope equilibrium exchange fractionation factors for various NOy molecules. Geochem. Cosmochim. Acta 164, 284–297.
Walters, W.W., Michalski, G., 2016. Theoretical calculation of oxygen equilibrium isotope fractionation factors involving various NO molecules, OH, and H_2O and its implications for isotope variations in atmospheric nitrate. Geochem. Cosmochim. Acta 191, 89–101.
Walters, W.W., Goodwin, S.R., Michalski, G., 2015a. Nitrogen stable isotope composition ($\delta^{15}N$) of vehicle-emitted NO*x*. Environ. Sci. Technol. 49, 2278–2285.
Walters, W.W., Tharp, B.D., Fang, H., Kozak, B.J., Michalski, G., 2015b. Nitrogen isotope composition of thermally produced NO*x* from various fossil-fuel combustion sources. Environ. Sci. Technol. 49, 11363–11371.
Wang, X., Wang, H., Xue, L., Wang, T., Wang, L., Gu, R., Wang, W., Tham, Y.J., Wang, Z., Yang, L.J., 2017. Observations of N_2O_5 and $ClNO_2$ at a polluted urban surface site in North China: high N_2O_5 uptake coefficients and low $ClNO_2$ product yields. Atmos. Environ. 156, 125–134.
Wang, Y., Li, W., Gao, W., Liu, Z., Tian, S., Shen, R., Ji, D., Wang, S., Wang, L., Tang, G., 2019. Trends in Particulate Matter and its Chemical Compositions in China from 2013–2017. Sci. China-Earth Sci., pp. 1–15
Wang, Y.L., Song, W., Yang, W., Sun, X.C., Tong, Y.D., Wang, X.M., Liu, C.Q., Bai, Z.P., Liu, X.Y., 2019. Influences of atmospheric pollution on the contributions of major oxidation pathways to $PM_{2.5}$ nitrate formation in Beijing. J. Geophys. Res. Atmos. 124, 4174–4185.
Womack, C., McDuffie, E., Edwards, P., Bares, R., de Gouw, J., Docherty, K., Dube, W., Fibiger, D., Franchin, A., Gilman, J.J.G.R.L., 2019. An odd oxygen framework for wintertime ammonium nitrate aerosol pollution in urban areas: NOx and VOC control as mitigation strategies. Geophys. Res. Lett. 46, 4971–4979.
Xu, W., Sun, Y., Wang, Q., Zhao, J., Wang, J., Ge, X., Xie, C., Zhou, W., Du, W., Li, J., Fu, P., Wang, Z., Worsnop, D.R., Coe, H., 2019. Changes in aerosol chemistry from 2014 to 2016 in winter in beijing: insights from high-resolution aerosol mass spectrometry. J. Geophys. Res. Atmos. 124, 1132–1147.
Zhang, Q., Zheng, Y., Tong, D., Shao, M., Wang, S., Zhang, Y., Xu, X., Wang, J., He, H., Liu, W., Ding, Y., Lei, Y., Li, J., Wang, Z., Zhang, X., Wang, Y., Cheng, J., Liu, Y., Shi, Q., Yan, L., Geng, G., Hong, C., Li, M., Liu, F., Zheng, B., Cao, J., Ding, A., Gao, J., Fu, Q., Huo, J., Liu, B., Liu, Z., Yang, F., He, K., Hao, J., 2019. Drivers of improved $PM_{2.5}$ air quality in China from 2013 to 2017. Proc. Natl. Acad. Sci. U.S.A.
Zhang, Z., Zeng, Y., Zheng, N., Luo, L., Xiao, H., Xiao, H., 2020a. Fossil fuel-related emissions were the major source of NH_3 pollution in urban cities of northern China in the autumn of 2017. Environ. Pollut. 113428.
Zhang, Z., Zheng, N., Liang, Y., Luo, L., Xiao, H., Xiao, H., 2020b. Dominance of heterogeneous chemistry in summertime nitrate accumulation: insights from oxygen isotope of nitrate ($\delta^{18}O-NO_3^-$). ACS. Earth Space Chem. 4, 818–824.
Zhang, Z., Zheng, N., Zhang, D., Xiao, H., Cao, Y., Xiao, H., 2020c. Rayleigh based concept to track NOx emission sources in urban areas of China. Sci. Total Environ. 135362.
Zhao, L., Wang, L., Tan, J., Duan, J., Ma, X., Zhang, C., Ji, S., Qi, M., Lu, X., Wang, Y., Wang, Q., Xu, R., 2019. Changes of chemical composition and source apportionment of PM2.5 during 2013–2017 in urban Handan, China. Atmos. Environ. Times 206, 119–131.
Zhou, W., Gao, M., He, Y., Wang, Q., Xie, C., Xu, W., Zhao, J., Du, W., Qiu, Y., Lei, L., Fu, P., Wang, Z., Worsnop, D.R., Zhang, Q., Sun, Y., 2019. Response of aerosol chemistry to clean air action in Beijing, China: insights from two-year ACSM measurements and model simulations. Environ. Pollut. 255.
Zong, Z., Wang, X., Tian, C., Chen, Y., Fang, Y., Zhang, F., Li, C., Sun, J., Li, J., Zhang, G., 2017. First assessment of NOx sources at a regional background site in North China using isotopic analysis linked with modeling. Environ. Sci. Technol. 51, 5923–5931.
Zong, Z., Tan, Y., Wang, X., Tian, C., Li, J., Fang, Y., Chen, Y., Cui, S., Zhang, G., 2020. Dual-modelling-based source apportionment of NOx in five Chinese megacities: providing the isotopic footprint from 2013 to 2014. Environ. Int. 137.